Structure and properties of polyamide 11 nanocomposites filled with fibrous palygorskite clay

Tech Science Press

Structure and Properties of Polyamide 11 Nanocomposites Filled with Fibrous Palygorskite Clay

B. Benobeidallah[1], A. Benhamida[1], A. Dorigato[2,*], A. Sola[3], M. Messori[3] and A. Pegoretti[2]

[1]Laboratoire des Matériaux Polymères Avancés (LMPA), Université Abderrahmane Mira de Bejaia, Bejaia, Algeria.

[2]Department of Industrial Engineering, University of Trento, Trento, Italy.

[3]Department of Engineering "Enzo Ferrari", University of Modena and Reggio Emilia, Modena, Italy.

[*]Corresponding Author: A. Dorigato. Email: andrea.dorigato@unitn.it.

Abstract: Various amounts (up to 10 wt%) of palygorskite nanofibers functionalized by 3-aminopropyltriethoxysilane (APTES) coupling agent were used to reinforce polyamide 11 nanocomposites prepared by melt compounding. The covalent bonding of the silane on the palygorskite surface was confirmed by infrared spectroscopy and thermogravimetric analysis. X-ray diffraction revealed the retention of the α-form of polyamide crystals upon the addition of both natural and silane treated palygorskite nanorods. All the investigated nanocomposites showed an improvement of the thermal stability, especially when surface treated palygorskite nanofibers were considered. Tensile tests and dynamic mechanical thermal analyses on the prepared materials evidenced how the incorporation of palygorskite nanofibers significantly increased the elastic and the storage moduli of polyamide, and this enhancement was more evident when natural palygorskite nanorods were used.

Keywords: Polyamide; clay; nanocomposites; thermal properties; mechanical properties

1 Introduction

In the recent years, there has been increasing interest for the development of nylon-based nanocomposites in both industry and academic areas. These new materials exhibit high-performances, including the enhancement of mechanical strength, stiffness and gas barrier properties with respect to the neat matrices. Therefore, these materials are interesting for various applications in the automotive and packaging fields. Furthermore, the properties of the resulting nanocomposites strongly depend on the organic matrix used, on the nanoparticles type and on the preparation techniques [1]. In particular, polyamide 11 (PA11) is a technical commercial polymer produced from renewable resources (i.e. castor oil). Thanks to its good chemical and barrier properties, excellent creep resistance and good ductility, PA11 has a great potential for future applications, including food packaging, automotive, electronics, biomedical. However, in many cases, its usage may be limited by its mechanical properties and thermal stability. In fact, several engineering applications require formulations stable both at room and at elevated temperatures with limited thermal degradation.

In the past years, many efforts have been devoted to improve the performances of PA11 by developing nanocomposites [2-8], mostly by the addition of inorganic materials of nanometric size. The results revealed an improvement of the mechanical, thermal and in flame retardant properties of the PA11 nanocomposites upon the addition of nanoparticles. For instance, Liu et al. [6] successfully prepared exfoliated nylon 11/organoclay nanocomposites, at low clay content, by melt compounding. A remarkable improvement in the thermal stability (about 20%) and mechanical properties for the exfoliated nanocomposites was obtained. He et al. [7] studied the rheological properties of PA11/clay nanocomposites prepared by melt blending. A steady increase of the storage modulus (G') and of the loss

modulus (G'') at low clay concentrations was detected, suggesting thus a more stable viscoelastic response for PA11/clay systems. Recently, Lao et al. [4,5] investigated the effect of different nanoparticles (i.e., nanoclays (NCs) and carbon nanofibers (CNFs)) on the flammability properties of PA11 and PA12 nanocomposites. The authors added an intumescent fire retardant (FR) additive to the nanofilled formulations, and the resulting composites exhibited higher decomposition temperature than the samples filled with solely FR additive.

In the present study, another kind of clay (i.e., palygorskite) was adopted as PA11 nanofiller. The palygorskite (PLG), also called attapulgite, is a crystalline hydrated magnesium aluminum silicate mineral containing ribbons of a 2:1 phyllosilicate structure. The palygorskite is characterized by a fibrous morphology [9,10]. In fact, the inversion of the tetrahedral sheet results in the discontinuity of the octahedral sheets, thus forming open channels of 3.7 Å x 6.4 Å along the fiber axis. Because of its special fibrous structure, higher aspect ratio, thermal/mechanical stability, and high density of silanol groups on the structural cavities [9], nowadays, palygorskite is attracting much attention in many areas of nanotechnology, especially in the preparation of polymer-clay nanocomposites [11-21]. However, single rod crystals of palygorskite usually exist as crystal bundles or aggregates owing to the electrostatic charge, the stronger hydrogen bonding and Van der Waals interaction between the fibers. Furthermore, the dispersion of PLG in non-polar matrices is a big challenge in the production of high-performance polymer/clay nanocomposites. In order to improve the dispersion degree and the interfacial adhesion of the nanofiller to low polar polymers, surface treatments of fibrous clays using silanes and other coupling agents have been widely investigated [14-18, 22]. Grafting organic compounds containing various groups on the surface of fibrous palygorskite through covalent bonds could improve the adhesion/compatibility with many polymeric matrices, and the strong anisotropy of these minerals could result in a significant reinforcing effect.

To the best of our knowledge, there have been no studies on the palygorskite fibrous clay as reinforcing and stabilizing nanofiller in polyamide 11. Therefore, in this paper a melt blending method was adopted to prepare nanocomposites with a polyamide 11 matrix. Both natural PLG and palygorskite functionalized with the 3-aminopropyltrietoxysilane were considered. This work represents the first step of a wider research activity aiming at the development of innovative nanofilled bioplastics, having elevated flame resistance and dimensional stability.

2 Experimental Part

2.1 Materials

Polymeric granules of PA11 were supplied by Arkema Specialty Polyamides (Colombes Cedex, France) under the trade name Rilsan® PA11 grade BESNO TL NB. The polymer was synthesized by a polycondensation reaction of 11-aminoundecanoic acid extracted from castor oil. The Rilsan® PA11 presents a density of 1.02 g/cm^3 and a melting point of 186 °C. Palygorskite nanofiber clay was extracted from Ghoufi's region situated in the North East of Algeria. The extracted palygorskite was subjected to mechanical and chemical treatments to remove impurities, such as dolomite and calcite. An acid chemical treatment was carried out with acetic acid solution (3M), and the residue was washed with distilled water to remove the acid from the clay. The sample was then dried at 80 °C overnight before grinding. The acid treatment allows the formation of a porous structure, to create a high surface area and to generate a high number of silanols group. Coupling agent 3-aminopropyltriethoxysilane(APTES) at 99% of purity was purchased from Sigma Aldrich.

2.2 Surface Treatment of Palygorskite

The silanization process of the palygorskite was performed according to the experimental protocol reported by Soberanis-Monforte et al. [19] in a paper on polyethylene/surface treated clay nanocomposites. A detailed description of this experimental procedure can be found in this paper. The silane coupling agent (APTES) was added into a palygorskite solution and stirred for 60 min at 40°C. In this case, an environmentally friendly solvent (i.e., distilled water) was utilized. According to the indication of the APTES producer, these are the recommended conditions to obtain a complete

solubilization of the silane molecules. The PLG concentration in the solution was 40 g/l. An excess of APTES of 10 wt% was utilized. In this way, the silane agent could condensate on the surface of PLG and forms a monolayer. The excess of 10 wt% represents the maximum quantity of APTES to reach an efficient grafting of the silane on the nanofiller surface, avoiding in the meanwhile the formation of multilayer organic structures, that could lead to the development of a weak interphase within the composite. The mixture was then centrifuged and the residue was washed with ethanol and distillated water to eliminate the excess of APTES. The solid material was dried in a vacuum oven at 80°C. Finally, the resulting silane surface treated palygorskite (sPLG) was ground and sieved. The size distribution of PLG and sPLG nanofillers after grinding was 50 μm.

2.3 Preparation of PA11 Nanocomposite Samples

Before being melt compounded, all the materials were dried overnight at 80°C, to eliminate the moisture and avoid the degradation of the polymer during melt processing. Different PA11/palygorskite nanocomposites containing 0, 1%, 3%, 5% and 10% by weight of both untreated (PLG) and silane surface treated (sPLG) palygorskite were prepared via melt blending in a Haake Rheomix® internal mixer. Polymer granules were introduced in the mixer, and after the complete melting of the PA11 (i.e., after 30 s), the nanofiller was added very slowly (i.e., in 30 s), to favor PLG dispersion within the matrix. During the process, the temperature in the mixing chamber was set at 225°C and a constant rotor speed of 60 rpm was selected. In this way, the partial rupture of the PLG aggregates and their distribution within the polymer matrix could be obtained. This mixing temperature was chosen to avoid the thermal degradation of the matrix during compounding and to make easier the removal of the material from the rotors. Also the rotor speed was selected to avoid the thermal degradation of the PA11. The resulting materials were then compression molded in a Carver hydraulic laboratory press at 225°C under a pressure of 7 tons for 10 minutes to obtain square sheets of composite samples with a thickness of around 1 mm. Also neat PA11 sample was processed following the same route.

2.4 Characterization Methods

2.4.1 Infrared Spectroscopy

To confirm the grafting of APTES on the palygorskite surface, the silanized palygorskite structure was investigated by Fourier Transform Infrared (FTIR) spectroscopy. The FTIR spectra of PLG and sPLG were obtained by a Perkin Elmer Spectrum One spectrometer. FTIR spectra were collected in a wavelength interval from 4000 cm^{-1} to 650 cm^{-1}. In this case the reflective spectroscopy was used, and thus the palygorskite powder was directly used.

2.4.2 Microscopic Examination (SEM)

Scanning Electron Microscopy (SEM) was carried out to evaluate the morphology of the PLG nanofibers before and after silanization and of the PA11/PLG nanocomposites. SEM images were acquired with a field emission scanning electron microscope (FESEM) Carl Zeiss AG Supra 40. The nanocomposite samples were cryogenically fractured in liquid nitrogen and the surfaces metallized with Pt-Pd.

2.4.3 X-Ray Diffraction Analysis

X-ray diffraction (XRD) analysis was employed in order to investigate the crystalline structure of the palygorskite, the polyamide 11 and of the relative nanocomposites samples. The X-ray diffraction patterns were acquired at room temperature by using an Xpert-PRO diffractometer system at a voltage of 40 kV and a current of 40 mA, equipped with an X'Celerator (PANalytical) detector. Experimental data were collected in a 2θ range from 5° to 60° at a 2θ step of 0.0167°, by using CuKα radiation (λ = 0.154 nm).

2.4.4 Surface Analysis

Specific surface area (SSA) of the palygorskite clay before and after silanisation was carried out by N_2 adsorption and desorption experiments at 77 K on a Micrometrics ASAP 2010 instrument. The N_2

isotherms were used to calculate the specific surface area, by applying the Brunauer-Emmett-Teller (BET) multipoint method.

2.4.5 Thermogravimetric Analysis (TGA)

The thermal stability of both PLG nanofillers and the PA11 nanocomposites was investigated through thermogravimetric analysis (TGA), by using a Mettler TGA Q5000 thermobalance under a nitrogen flow of 15 ml/min in a temperature interval from 25°C to 700°C, at a heating rate of 10 °C/min. In this way, the temperature associated to a mass loss of 10% ($T_{10\%}$), the decomposition temperature T_d (i.e., the temperature associated to the maximum mass loss rate) and the residue at 700°C (m_{700}) were determined.

2.4.6 Differential Scanning Calorimeter (DSC)

The thermal behavior of the prepared nanocomposites was investigated with a Mettler® DSC30 differential scanning calorimeter. All measurements were performed according to a heat/cool/heat thermal cycle in a temperature range from 0°C to 250°C at a heating/cooling rate of 10 °C/min, under a nitrogen flow (N_2) of 150 ml/min. In this way, the glass transition temperature (T_g), the melting temperature (T_m), the crystallization temperature (T_c) and the melting enthalpy (ΔH_m) were determined. In addition, the crystalline fraction (X_c) of the samples was determined according to Eq. (1),

$$Xc = \frac{\Delta H_m}{\Delta H_0(1-\varphi)} \quad (1)$$

where ΔH_m is the melting enthalpy (J/g), ΔH_0 represents the theoretical melting enthalpy of 100% crystalline PA11, equal to 206 J/g [3], and φ corresponds to the nanofiller weight fraction of PLG clay in the nanocomposites.

2.4.7 Viscoelastic Behavior in the Molten State

The melt flow index was also measured following the ASTM D1238 standard with a melt indexer Dynisco LMI 4000 Series. These tests were conducted at a fixed temperature of 230°C, applying a load of 5.0 kg.

2.4.8 Tensile Tests

Quasi-static tensile tests were carried out on ISO 527 type 1BA dumbbells (gage length 30 mm, width 5 mm) by using an Instron® 4502 tensile machine equipped with a load cell of 100 N at a cross-head speed of 50 mm/min. In this way, the stress at break (σ_b) and strain at break (ε_b) were determined. The elastic modulus (E) was evaluated as secant modulus between deformation levels of 0.05% and 0.25%, according to ISO 527 standard, by using a resistance extensometer Instron® model 2620-601 (gage length = 12.5 mm). The tests were performed at a crosshead speed of 0.25 mm/min, imposing a maximum axial deformation level of 1%. At least five specimens were tested for each composition.

2.4.9 Dynamic Mechanical Analysis (DMA)

Dynamic mechanical analysis was performed in order to investigate the thermo-mechanical behaviour of the nanocomposites. All measurements were performed by using a DMA Q800 instrument, testing rectangular samples with dimensions of 13 × 5 × 1 mm^3, in a temperature range from 0°C to 150°C, at a heating rate of 3 °C/min and at a frequency of 1 Hz. In this way, dynamic storage moduli (E', E'') and the damping factor (tanδ) data were collected.

3 Results and Discussion

3.1 Structural and Morphological Characterization of PLG and sPLG

The FTIR spectra of the original PLG and of the silanized palygorskite (sPLG) are shown in Fig. 1. New absorption bands can be detected in the sPLG sample, at 2927 cm^{-1} and 3270 cm^{-1} attributed to C-H and N-H stretching vibrations of the silane, respectively [19,23]. These bands indicate a covalent link between APTES molecules and PLG nanofibers. The bands appearing in PLG sample, at 3620 cm^{-1}, 3540

cm^{-1} and 3390 cm^{-1} can be assigned to the stretching vibration of the hydroxyls Al-OH, Mg-OH and zeolitic water, respectively, in the fibrous structure [19,20,24]. As shown in Fig. 1, the intensities of these bands are weakened after the grafting process of the APTES, suggesting that a substitution reaction occurred between APTES molecules and the O-H groups on the surface of the palygorskite. Similar results were previously reported by other authors in literature [22,24]. It can be therefore concluded that the silane surface modification of PLG nanofiller was successfully performed.

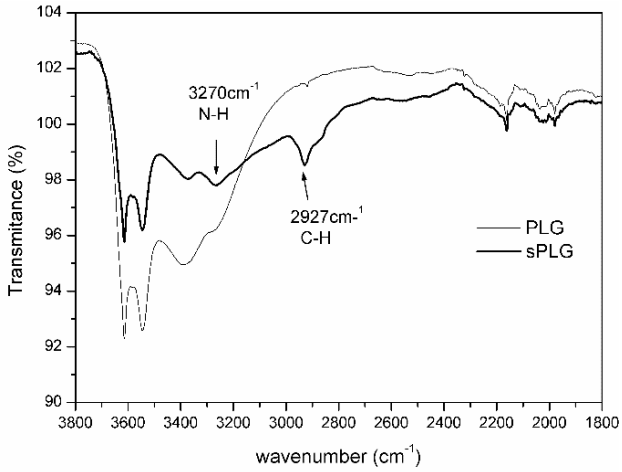

Figure 1: FTIR spectra of PLG and sPLG nanofillers

The XRD patterns of the PLG and sPLG are shown in Fig. 2. The main characteristic reflection peak at 2θ~8.4° is attributed to the basal plane (110). Other reflections at 13.8°, 19.8° and 26.5°, corresponding to the (200), (040) and (400) plane in the structure of the PLG, can be also detected [12,15]. It can be observed that the XRD diffractogram of palygorskite is not affected by the treatment with APTES molecules, indicating that the silane grafting does not alter the crystalline structure of the fibrous palygorskite. This result finds confirmation in the conclusions previously reported by various authors [16,18,20,22,25].

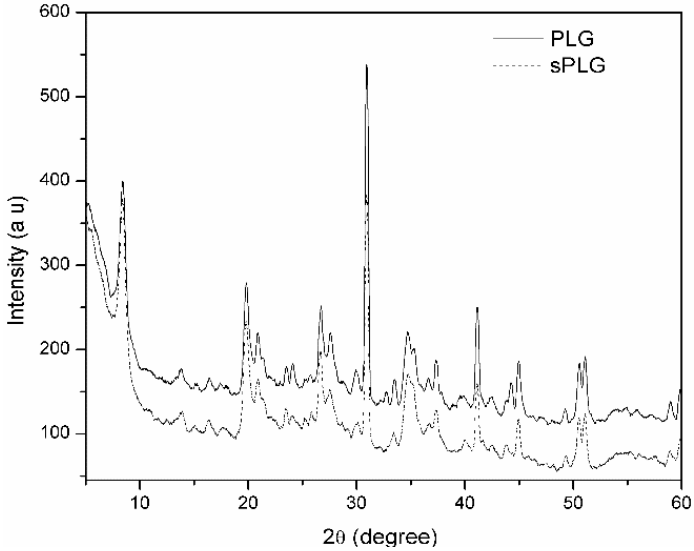

Figure 2: X-Ray diffraction patterns of PLG and sPLG nanofillers

As reported in Figs. 3(a)-3(b), SEM observation clearly shows that the untreated palygorskite presented a fibrous morphology, in which aggregates of entangled rods randomly oriented can be detected. This was due to the strong interactions existing between the fibrous crystals, which makes it difficult to find single fiber crystals. After chemical treatment, the aggregates were separated and the fibers seemed to be more dispersed and less compacted in the silanized palygorskite with more open pores. In fact, the organic molecules grafted on the surface of rod-like crystals can reduce the surface energy and the interactions between the single fibers. Similar morphologies were also reported in the literature where large aggregates can be broken down to single fibers after organic modification [17,21]. However, the morphological differences between PLG and sPLG nanofillers are not so much pronounced, and further analysis with TEM will be performed in the future to better highlight the different microstructure of these materials.

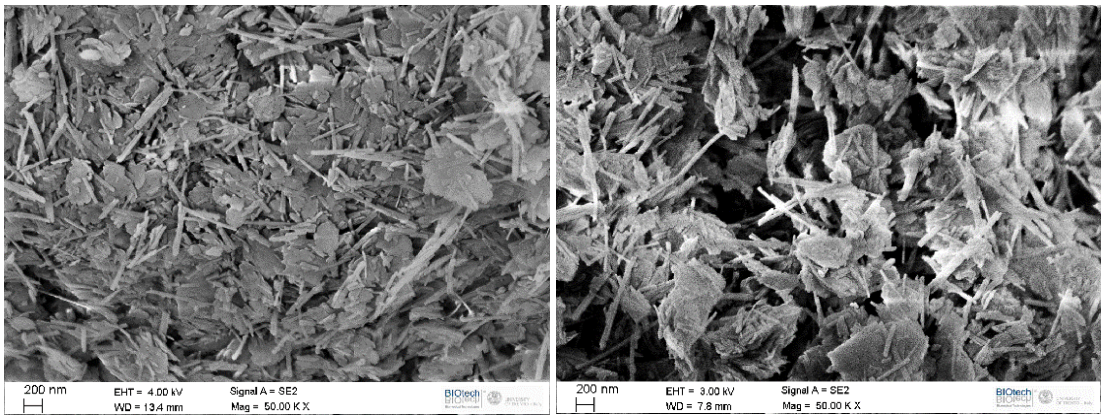

(a) (b)

Figure 3: SEM images of the (a) PLG and (b) sPLG nanofillers

Figs. 4(a)-4(b) illustrate the thermogravimetric curves of PLG and sPLG nanorods. According to these figures, a continuous mass loss can be observed for both samples. PLG showed its first mass loss at 50-70°C attributed to the removal of physisorbed water in the palygorskite surface. The mass loss steps at 180°C and 486°C can be ascribed to the elimination of zeolitic water from the channels and of the coordinated water in the fibrous structure, respectively. The mass loss at 628°C is assigned to the dihydroxylation of the palygorskite [11,25]. As reported in Fig. 4(b), the sPLG sample shows a similar mass loss trend with respect to the natural PLG, but additional endothermic events at 284°C and 408°C, both assigned to the thermal decomposition of grafted carbon chains of the organosilane, can be detected [18,26,27]. These results further confirm that the grafting of APTES on the palygorskite surface was successfully performed. BET method reveals that the specific surface area decreases after the surface treatment of the PLG nanoparticles, from 82 m^2/g to 45 m^2/g for natural PLG and sPLG, respectively, suggesting that the organic molecules may block the pores/tunnels, with a consequent decrease of the N_2 accessibility [28].

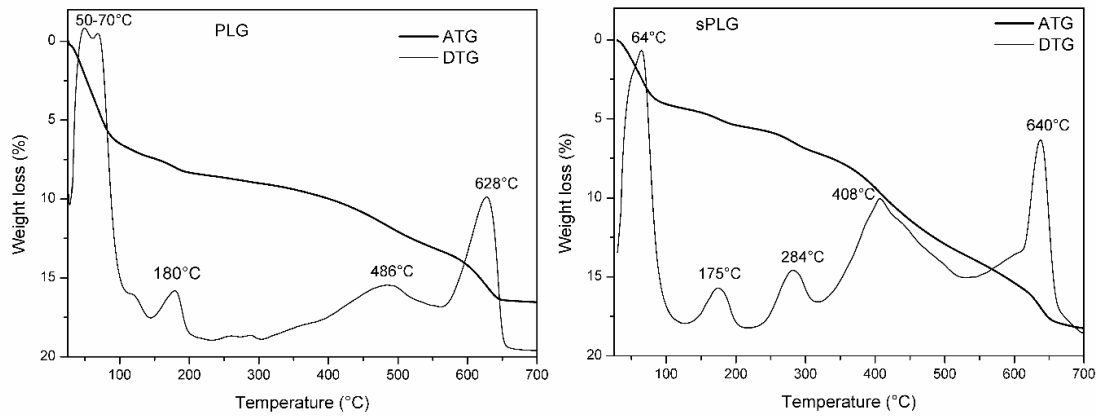

Figure 4: Thermogravimetric curves of (a) PLG and (b) sPLG nanofillers

3.2 Morphological and Structural Properties of PA11 Nanocomposites

The morphology of polymer nanocomposites plays an important role on their physico-mechanical properties. The dispersion of palygorskite nanoparticles and the interfacial bonding were investigated through SEM analysis of the cryofractured surfaces of nanocomposite films. SEM images of the nanocomposites filled with both natural and silanized palygorskite at 5 wt% content are reported in Figs. 5(a)-5(c). Randomly distributed palygorskite aggregates of nanometric size (<100 nm) can be noticed in the PA11/PLG5%wt sample (Fig. 5(b)), indicating a poor dispersion of the PLG single fibers in the polymer matrix probably due to the strong interparticle interactions and the weak filler/matrix compatibility. On the contrary, in PA11/sPLG5wt% sample few agglomerates with low diameter and a rougher surface can be detected. This observation proves the development of stronger interactions between the silanized palygorskite and the PA11, as a result of the presence of the organic chains on the surface of the PLG nanoparticles. These results evidenced the effectiveness of nanofiller surface treatment on its dispersion degree in the resulting nanocomposites.

XRD patterns of PA11 and its nanocomposites filled with 5 wt% of PLG and sPLG are reported in Fig. 6. Neat PA11 sample exhibits three characteristic peaks at diffraction angles of around $2\theta = 7.23°$, 20.23° and 23°, respectively associated to the (001), (100) and (010/110) plane, indicating the presence of the triclinic α-form of nylon 11 [6,29,30]. Unlike layered clays, whose primary diffraction peaks shift significantly to higher/lower angles when it is aggregated/exfoliated in a polymer matrix [31], the unit layer in a single rod crystal cannot be separated or delaminated, because this would imply the disruption of the silicate structure. Therefore, the characteristic diffraction peak of the PLG nanofiller, located at $2\theta = 8.4°$, keeps its original position even if the PLG is well dispersed in the matrix [12,18,32]. For this reason, it is difficult to evaluate the nanofiller dispersion in these nanocomposites by using XRD technique. Therefore, it can be concluded that the addition of both PLG and sPLG does not markedly affect the crystalline morphology of the PA11 matrix that crystallizes in its thermodynamically stable triclinic α-form.

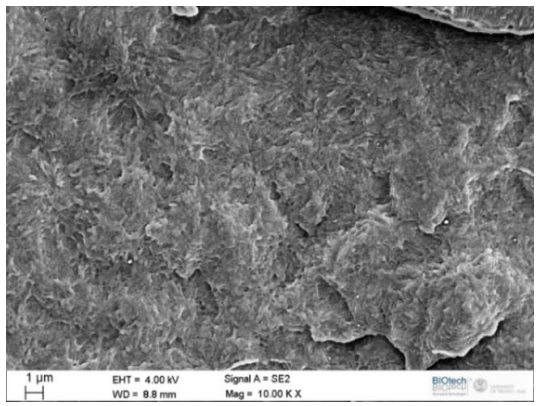

(a)

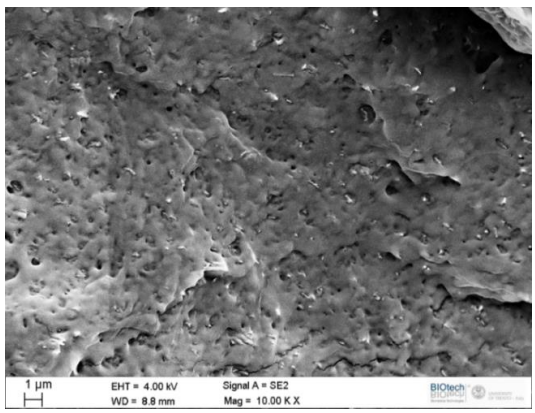

(b)

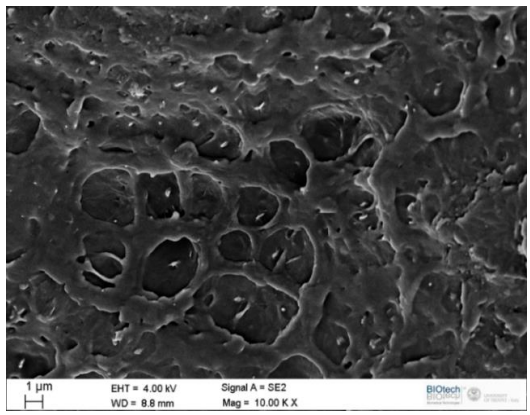

(c)

Figure 5: SEM micrographs of the cryofractured surface of (a) neat PA11, (b) PA11/PLG 5%wt and (c) PA11/sPLG5%wt nanocomposites

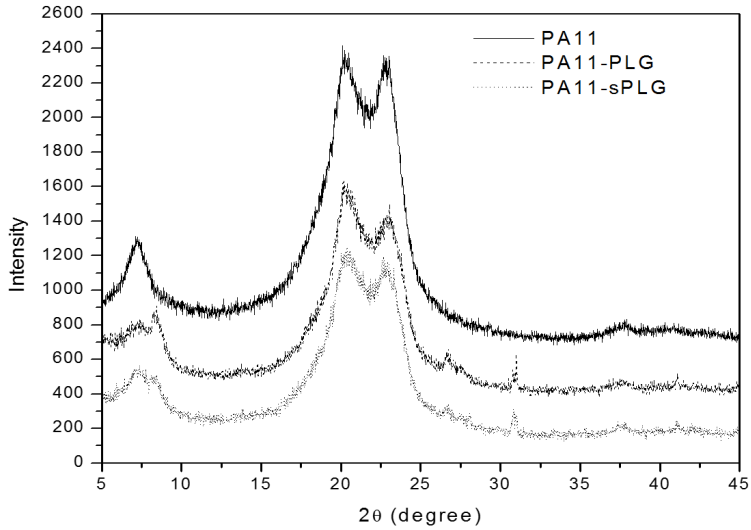

Figure 6: XRD patterns of PA11 and its nanocomposites at a filler content of 5 wt%

3.3 Thermal Properties of the Nanocomposites

The crystallization behaviour is one of the most important aspects to determine the properties of the PA11/PLG nanocomposites [33] and therefore neat PA11 and the corresponding nanocomposites at different nanofiller concentrations were characterized by DSC. The most important thermal properties collected from DSC during second heating and cooling scan (i.e., glass transition temperature (T_g), melting temperature (T_m) and crystallization temperature (T_c)) are listed in Table 1. For the data reported in this table, it can be concluded that both T_m and T_g are not substantially affected by nanofiller addition. Interestingly, both PLG and sPLG seem to play a nucleating effect on the PA11 matrix. In fact, both the crystallization temperature (T_c) and the crystallinity degree (X_c) are slightly increased upon nanofiller addition. A similar result was already detected by Dorigato et al. on PA6 nanocomposites [34].

Table 1: Results of DSC and TGA tests on neat PA11 and its relative nanocomposites

	T_g (°C)	T_m (°C)	T_c (°C)	X_c (%)	$T_{10\%}$ (°C)	T_d (°C)	m_{700} (%)
Neat PA11	39.2	187.2	163.2	22.5	415.4	453.0	0.3
PA11/PLG-1wt%	39.5	187.0	164.0	23.3	423.0	463.0	0.7
PA11/PLG-3 wt %	39.5	187.1	164.7	24.0	427.0	465.0	2.8
PA11/PLG-5wt%	39.6	188.6	165.4	25.7	428.0	464.0	3.9
PA11/PLG-10wt%	40.2	190.5	166.4	23.0	429.0	467.0	8.5
PA11/sPLG-1wt%	40.3	188.0	163.3	22.6	424.3	460.0	1.0
PA11/sPLG-3wt%	40.5	187.4	163.4	23.1	430.0	464.0	2.4
PA11/sPLG-5wt%	40.6	188.4	163.1	23.8	436.0	469.0	4.1
PA11/sPLG-10wt%	41.9	189.7	165.9	25.7	438.0	469.0	7.5

TGA in nitrogen atmosphere was carried out in order to investigate the thermal stability of the PA11 nanocomposites filled with different PLG loadings. In Tab. 1 the temperatures associated with a mass loss of 10% ($T_{10\%}$), the decomposition temperature (T_d) and the mass residue at 700°C (m_{700}) are reported. It is interesting to note how both $T_{10\%}$, T_d and m_{700} values of nanofilled samples are higher than that of the neat PA11. Therefore, the PA11/PLG and PA11/sPLG nanocomposites present a relatively good thermal stability, especially at elevated filler amounts. As already explained in a previous work of our group [35], the improvement of the thermal stability is due to the barrier effect of the fibers, which act as heat insulator and mass transport barrier, hindering the development and the diffusion of the volatile decomposition products [8,15,33]. Compared to PA11/PLG, PA11/sPLG nanocomposites show a better thermal stability for all the investigated compositions. For instance, the decomposition temperature at 10% weight loss increases from 415°C for neat PA11 up to 429°C and 438°C for PA11 filled with 10 wt% of PLG and of sPLG, respectively. This difference could be probably attributed to a better nanofiller dispersion of organomodified PLG within the polymer matrix. Moreover, the residue at 700°C (m_{700}) left after combustion of neat PA11 is nearly zero, as all the organic components of the matrix decompose into gaseous products, while the remaining mass at 700°C of the nanofilled samples corresponds to the palygorskite nanoparticles mass percentage.

3.4 Thermo-Mechanical Properties of the Nanocomposites

Fig. 7(a) shows the trends of the elastic modulus for the PA11 based nanocomposites. It can be seen that the elastic modulus of the nanocomposites monotonically increases with the filler content, and the increase is more pronounced for nanocomposites with untreated palygorskite (+21% with a PLG content of 10 wt%). As already reported in literature [36,37], such increase of the elastic modulus is probably due to the efficient interfacial stress transfer of the nanofibers. It is also probable that fibrous morphology with a high aspect ratio of this mineral is a crucial point in reinforcement for these nanocomposite systems [32,38]. It is interesting to note how the presence of the APTES silane agent on the surface of PLG slightly limits the elastic modulus increase with respect to the untreated PLG filled samples. This result could be attributed to the decrease of the specific surface area of the PLG, as identified by structural

analysis, after the incorporation of the silane agent. It can be also hypothesized that the APTES molecules act as a plasticizer at the polymer-nanofiller interface, reducing thus the stiffening action played by PLG. Moreover, at elevated filler concentrations it should also be considered that both PLG and sPLG nanofillers can form a percolating network, with a consequent increase of the material stiffness. However sPLG nanofiller, having covered partly its surface with the silane, is inhibited to form such strong structure, since less surface and less polar sites are available to establish a strong contact between the particles.

The effect of the PLG nanorods on the tensile strength and the elongation at break is shown in Figs. 7(b)-7(c). As reported in Fig.7(b), the tensile strength is slightly reduced upon addition of PLG nanorods, and only with the incorporation of 1 wt% of sPLG σ_b values are slightly increased (about 10%). On the other hand, the elongation at break of the neat PA11 is 353 %, but this value increases to 366% and 420% after the incorporation of 1 wt% of PLG and sPLG nanoparticles, respectively (see Figure 7c). A further increase of the nanofiller content results in a heavy decrease of the elongation at break, probably because of the nanofiller aggregation at elevated concentrations. Furthermore, a closer examination of the curves indicates that both σ_b and ε_b values of the PA11/sPLG systems are systematically higher than those registered for PA11/PLG nanocomposites. This is probably due to the better nanofiller dispersion within the PA11 matrix obtained upon PLG silanization.

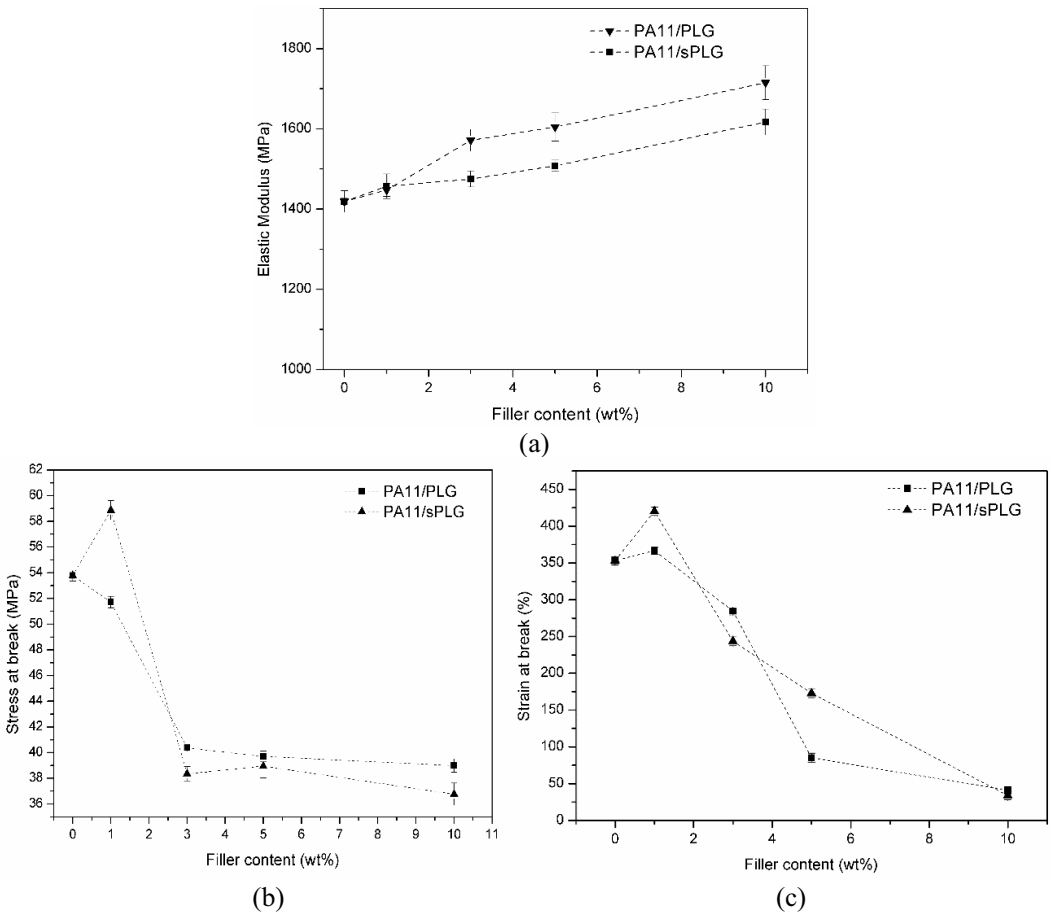

Figure 7: (a) Elastic modulus, (b) stress at break and (c) strain at break of the nanocomposites as a function of the palygorskite content

Dynamic mechanical properties (DMA) were investigated to characterize the thermo-mechanical properties of the nanocomposites at the solid state. Figs. 8(a)-8(b) report the trends of the dynamic storage modulus (E') of the nanocomposites as a function of temperature. It can be easily seen that, as the nanofiller content increases, the storage modulus steadily increases over the whole range of the testing temperatures. The examination of the storage modulus curves highlights how the enhancement of the storage modulus values is more pronounced at higher temperature, where the polymer matrix is more compliant and the stiffening effect played by the nanofiller is more effective. For instance, at 20°C the E' value of the neat PA11 (i.e., 1605 MPa) is increased at 2000 MPa (+24.6%) and 1890 MPa (+17.8%) for PA11-PLG-10 and PA11-sPLG-10 nanocomposites, respectively. At 90°C, the E' of the neat PA11 (i.e., 270 MPa) is respectively enhanced at 400 MPa (+48.1%) and 390 MPa (+44.4%) for PA11-PLG-10 and PA11-sPLG-10 nanocomposites. According to the results of quasi-static tensile tests, it can be noticed that the increase of the storage modulus for PA11/sPLG nanocomposites is less evident than that measured for nanocomposites containing neat PLG. For instance, the storage modulus at 0°C is increased by 8 % and 15% with the addition of 5 wt% of sPLG and PLG nanofibers, respectively. It can be therefore hypothesized that the presence of a soft organic interphase around the PLG nanofiller limits its stiffening capability. The evolution of the damping factor (tanδ) versus temperature of the nanocomposite samples is presented in Figs. 9(a)-9(b). The damping factor progressively decreases upon nanofiller addition, and also in this case the stiffening effect played by PLG nanoparticles is more evident than that played by sPLG nanofiller. Moreover, the position of the tanδ peak (i.e., the T_g of the material) is not substantially influenced by the nanofiller addition, confirming the results coming from DSC tests.

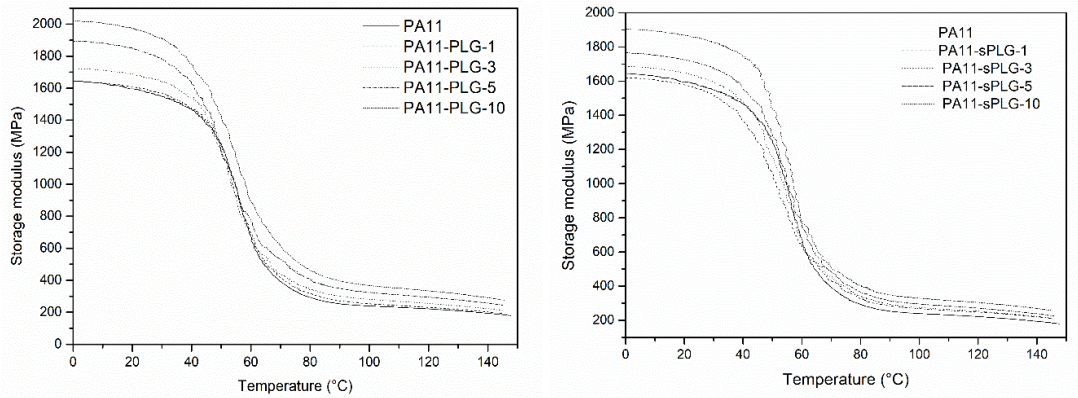

(a) (b)

Figure 8: Storage modulus (E') versus temperature of PA11 and its relative nanocomposites, (a) PLG filled and (b) sPLG filled samples

In order to have information on the effect of the PLG nanorods on the viscosity (i.e., the processability) of the nanocomposites, the melt flow index (MFI) was also evaluated. The trends of the MFI of the neat PA11 and the relative nanocomposites are reported in Fig. 10. As often happens with nanofilled samples [39], a general reduction of the MFI with the increase of the nanofillers loading can be observed. This result indicates an increase in the viscosity of the PA11 with the palygorskite loadings, which is probably due to the good interaction between the matrix and silicate fibers and between PLG particles, leading to the restriction of molecular mobility of polymeric segments near the silicate surface. Indeed, this decrease is more pronounced for the PA11/sPLG nanocomposites (at least for filler loadings up to 5 wt%), indicating probably a higher interfacial adhesion between the polyamide matrix and the silanized palygorskite. However, the decrease of the MFI, even if important (from 27.0 g/10 min up to 9.2 g/10 min with a PLG amount of 10 wt%), is not dramatic, and the material retains an acceptable processability even at elevated filler concentrations.

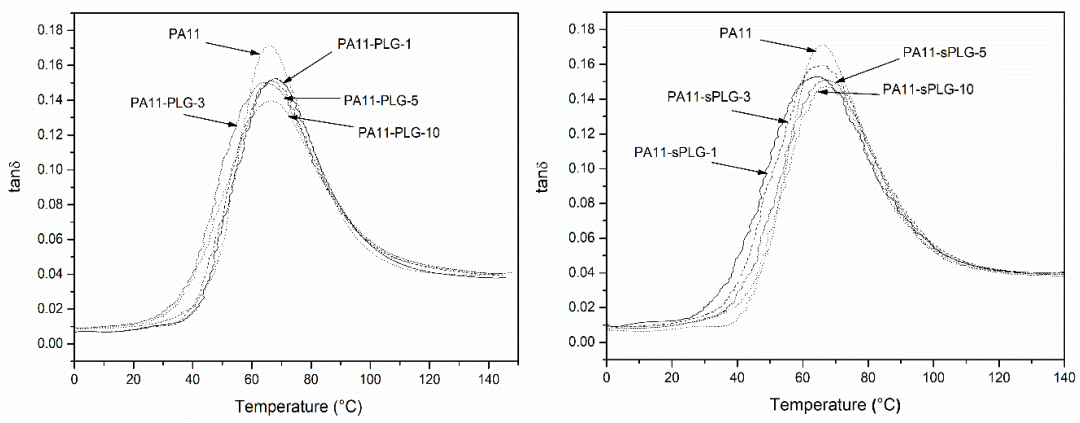

(a) (b)

Figure 9: Loss tangent (tanδ) of PA11 and its relative nanocomposites, (a) PLG filled and (b) sPLG filled samples

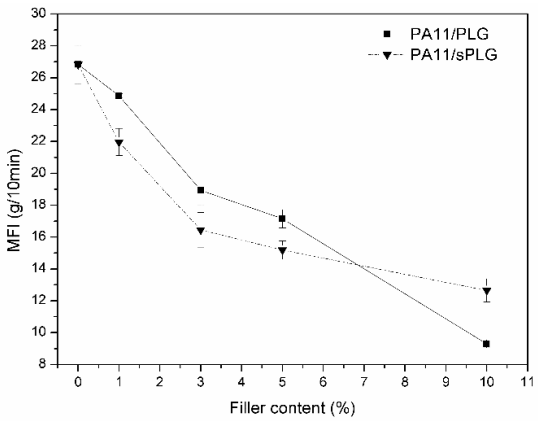

Figure 10: Melt flow index of PA11/PLG and PA11/sPLG nanocomposites at various nanofiller contents

4 Conclusions

In this work, PA11 nanocomposites containing a fibrous clay (i.e. palygorskite), were prepared via melt blending at different concentrations. The effect of PLG silanization on the physical properties of the resulting materials was also investigated. X-ray diffraction analysis demonstrated how the formation of α-form crystals of PA11 could be maintained even after the addition of both natural (PLG) and silane treated (sPLG) palygorskite nanorods, while DSC evidenced a nucleating effect played by palygorskite introduction, with an increase of the crystallization temperature and the crystallinity degree with respect to the neat PA11. Thermal stability was interestingly improved, especially at elevated filler amounts. Tensile tests and dynamic mechanical analyses on the prepared materials evidenced how the incorporation of palygorskite nanofibers significantly increased the stiffness of the prepared materials, especially when the untreated nanofiller is used. As a drawback, tensile properties at break were reduced. It was therefore demonstrated the potential of this nanofiller in increasing the thermo-mechanical stability of PA11 based bioplastic products.

References

1. Dorigato A, Brugnara M, Pegoretti A. Novel polyamide 12 based nanocomposites for industrial applications. *Journal of Polymer Research* **2017**, 24: 96.

2. Wu M, Yang G, Wang M, Wang W, Zhang W, Feng J, Liu T. Nonisothermal crystallization kinetics of ZnO nanorod filled polyamide 11 composites. *Materials Chemistry Physics* **2008**, 109: 547-555.
3. Mago G, Kalyon DM, Fisher FT. Nanocomposites of polyamide-11 and carbon nanostructures: Development of microstructure and ultimate properties following solution processing. *Journal of Polymer Science Part B: Polymer Physics* **2011**, 49: 1311-1321.
4. Lao SC, Wu C, Moon TJ, Koo JH, Morgan A, Pilato L, Wissler G. Flame retardant polyamide11 and 12 nanocomposites: thermal and flammability properties. *Journal of Composite Materials* **2009**, 43: 1803-1818.
5. Lao SC, Koo JH, Moon TJ, Londa M, Ibeh CC, Wissler GE, Pilato LA. Flame-retardant polyamide 11 nanocomposites: further thermal and flammability studies. *Journal of Fire Sciences* **2011**, 29(6).
6. Liu T, Lim KP, Tjiu WC, Pramoda KP, Chen ZK. Preparation and characterization of nylon 11/organoclay nanocomposites. *Polymer* **2003**, 44: 3529-3535.
7. He X, Yang J, Zhu L, Wang B, Sun G, Lv P, Phang IY, Liu T. Morphology and Melt Rheology of Nylon 11/Clay Nanocomposites. *Journal of Applied Polymer Science* **2006**, 102: 542-549.
8. Zhang X, Yang G, Lin J. Synthesis, rheology, and morphology of Nylon-11/Layered silicate nanocomposite. *Journal of Polymer Science Part B: Polymer Physics* **2006**, 44: 2161-2172.
9. Galan E. Properties and applications of palygorskite-sepiolite clays. *Clay Minerals* **1996**, 31: 443-453.
10. Brigatti MF, Galan E, Theng BKG, Modena I. Structures and mineralogy of clay minerals. *Handbook of Clay Science* **2006**, 1: 19-86.
11. Ruiz-hitzky E, Darder M, Fernandes FM, Wicklein B, Alcântara ACS, Aranda P. Progress in Polymer Science Fibrous clays based bionanocomposites. *Progress in Polymer Science* **2013**, 38: 1392-1414.
12. Pan B, Yue Q, Ren J, Wang H, Jian L, Zhang J, Yang S. A study on attapulgite reinforced PA6 composites. *Polymer Testing* **2006**, 25: 384-391.
13. Zhao L, Du QIN, Jiang G, Guo S. Attapulgite and ultrasonic oscillation induced crystallization behavior of polypropylene. *Journal of Polymer Science Part B: Polymer Physics* **2007**, 45: 2300-2308.
14. Chen J, Chen J, Zhu S, Cao Y, Li H. Mechanical properties, morphology, and crystal structure of polypropylene /chemically modified attapulgite nanocomposites. *Journal of Applied Polymer Science* **2011**, 121: 899-908.
15. Chen L, Liu K, Jin TX, Chen F, Fu Q. Rod like attapulgite/poly (ethylene terephthalate) nanocomposites with chemical bonding between the polymer chain and the filler. *eXPRESS Polymer Letters* **2012**, 6: 629-638.
16. Wang L, Sheng J. Preparation and properties of polypropylene/org-attapulgite nanocomposites. *Polymer* **2005**, 46: 6243-6249.
17. Shen L, Lin Y, Du Q, Zhong W, Yang Y. Preparation and rheology of polyamide-6/attapulgite nanocomposites and studies on their percolated structure. *Polymer* **2005**, 46: 5758-5766.
18. Yuan X, Li C. Guan G, Liu X, Xiao Y, Zhang D. Synthesis and Characterization of Poly(ethylene terephthalate)/Attapulgite Nanocomposites. *Journal of Applied Polymer Science* **2007**, 103(2): 1279-1286.
19. Soberanis-Monforte GA, Gonzalez-Chi PI, Gordillo-Rubio JL. Influence of chemically treated palygorskite over the rheological behavior of polypropylene nanocomposites. *Ingeniería, Investigación y Tecnología* **2015**, 16: 491-501.
20. Wang C, Wu Q, Liu F, An J, Lu R, Xie H, Cheng R. Synthesis and characterization of soy polyol-based polyurethane nanocomposites reinforced with silylated palygorskite. *Applied Clay Science* **2014**, 101: 246-252.
21. Zhang Y, Yu C, Hu P, Tong W, Lv F, Chu PK, Wang H. Mechanical and thermal properties of palygorskite poly (butylene succinate) nanocomposite. *Applied Clay Science* **2016**, 119: 96-102.
22. Xue S, Reinholdt M, Pinnavaia TJ. Palygorskite as an epoxy polymer reinforcement agent. *Polymer* **2006**, 47: 3344-3350.
23. Zhang Y, Zhao J, Chu H, Zhou X, Wei Y. Effect of modified attapulgite addition on the performance of a PVDF ultra filtration membrane. *Desalination* **2014**, 344: 71-78.
24. Boudriche L, Calvet R, Hamdi B, Balard H. Effect of acid treatment on surface properties evolution of attapulgite clay : An application of inverse gas chromatography. *Colloids and Surfaces A : Physicochemical and Engineering Aspects* **2011**, 392: 45-54.
25. Moreira MA, Ciuf KJ, Rives V, Vicente MA, Trujillano R, Gil A, Korili SA, De Faria EH. Effect of chemical modification of palygorskite and sepiolite by 3-aminopropyltriethoxisilane on adsorption of cationic and anionic dyes. *Journal of Applied Polymer Science* **2017**, 135: 394-404.
26. Liu P, Zhu L, Guo J, Wang A, Zhao Y, Wang Z. Palygorskite/polystyrene nanocomposites via facile in-situ bulk polymerization : Gelation and thermal properties. *Applied Clay Science* **2014**, 100: 95-101.
27. Zhu L, Guo J, Liu P, Zhao S. Novel strategy for palygorskite/poly (acrylic acid) nanocomposite hydrogels from bi-functionalized palygorskite nanorods as easily separable adsorbent for cationic basic dye. *Applied*

Clay Science **2016**, 121-122: 29-35.
28. Xi Y, Mallavarapu M, Ravendra N. Adsorption of the herbicide 2,4-D on organo palygorskite. *Applied Clay Science* **2010**, 49: 255-261.
29. Hu G, Ding Z, Li Y, Wang B. Crystalline morphology and melting behavior of nylon11/ethylene-vinyl alcohol /dicumyl peroxide blendszs. *Journal of Polymer Research* **2009**, 16: 263-269.
30. Fornes TD, Paul DR. Structure and properties of nanocomposites based on nylon-11 and-12 compared with those based on nylon-6. *Macromolecules* **2004**, 37: 7698-7709.
31. Zhang X, Yang G, Lin J. Crystallization Behavior of Nylon 11/Montmorillonite Nanocomposites Under Annealing. *Journal of Applied Polymer Science* **2006**, 102: 5483-5489.
32. Ruiz-Hitzky E, Darder M, Fernandes FM, Wicklein B, Alcântara ACS, Aranda P. Fibrous clays based bionanocomposites. *Progress in Polymer Science* **2013**, 38: 1392-1414.
33. Sinha Ray S, Okamoto M. Polymer/layered silicate nanocomposites: a review from preparation to processing. *Progress in Polymer Science* **2003**, 28: 1539-1641.
34. Dorigato A, Brugnara M, Giacomelli G, Fambri L, Pegoretti A. Thermal and mechanical behavior of innovative melt-blown fabrics based on polyamide nanocomposites. *Journal of Industrial Textiles* **2016**, 45(6).
35. Dorigato A, Pegoretti A, Frache A. Thermal stability of high density polyethylene-fumed silica nanocomposites. *Journal of Thermal Analysis and Calorimetry* **2012**, 109(2).
36. Dorigato A, Amato MD, Pegoretti A. Thermo-mechanical properties of high density polyethylene-fumed silica nanocomposites : Effect of filler surface area and treatment. *Journal of Polymer Research* **2012**, 19: 9889.
37. Dorigato A, Sebastiani M, Pegoretti A, Fambri L. Effect of silica nanoparticles on the mechanical performances of poly (lactic acid). *Journal of Polymers and the Environment* **2012**, 20: 713-725.
38. Yin H, Chen H, Chen D. Morphology and mechanical properties of polyacrylonitrile/attapulgite nanocomposite. *Journal of Materials Science* **2010**, 45: 2372-2380.
39. Dorigato A, Pegoretti A, Penati A. Linear low-density polyethylene/silica micro- and nanocomposites: dynamic rheological measurements and modelling. *eXPRESS Polymer Letters* **2010**, 4: 115-129.